

Supplement of

Contrasting Air Pollution Responses to Hourly Varying Anthropogenic NO_x Emissions in the Contiguous United States

Madankui Tao et al.

Correspondence to: Madankui Tao (taoma528@mit.edu)

Contents of this file

Text S1 to S5
Figures S1 to S12
Tables S1 to S5

Text S1. Interpreting the BASE Case: Sensitivity to Emissions Perturbations and Alternative Chemistry

To optimize computational resources while still identifying key sensitivities, we perform five simulations over five days from July 1 to July 5, 2018 (Table S1). We conduct three simulations to evaluate model responses to major sources of precursors, including 1) a 30% reduction in total anthropogenic emissions (hereafter referred to as *CAMS_m30anthro*) by modifying the anthropogenic emissions files; 2) a 30% reduction in total biogenic emissions (*CAMS_m30bio*) by scaling MEGAN emission factors to 0.7; and 3) the implementation of the MOZART-TS2 chemical mechanism (*CAMS_chemTS2*) by changing the model component set, which incorporates more comprehensive gas-phase chemistry for isoprene and terpenes (Schwantes et al., 2022). Analysis of these simulations provides context for evaluating changes in concentrations and chemical sensitivity driven by the incorporation of the regional 2017 U.S. National Emissions Inventory (NEI) adjusted for July 2018 simulation and by differences in the temporal resolution of anthropogenic emissions. The selected 30% perturbation for emission sources allows us to detect signals while maintaining relevance for scaling linearly to 100% (Turnock et al., 2018; Wild et al., 2012; S. Wu et al., 2009).

Overall, the emission perturbation simulations indicate that pollutants decrease with reductions of their dominant sources, as expected. A 30% reduction in total anthropogenic emissions leads to regional average decreases in all pollutants: surface NO₂ concentrations decrease by 20-24% (0.3-0.6 ppb; range reflects the average concentrations in six different regions), O₃ by 2.6-7.5% (1.1-3.5 ppb), HCHO by about 5.0% (0.1-0.4 ppb), CO by 3.1-6.6% (3.7-10 ppb), SO₂ by 19-25% (0.1-0.6 ppb), and PM_{2.5} by 1.7-5.4% (0.1-0.7 μg/m³) (Figs. S1 and S2). The largest reductions in NO₂ and CO occur in areas where emissions of these pollutants are largest (Fig. S4b). The Northeast region shows the largest decreases in O₃, surface NO₂ and HCHO, while the western CONUS experiences the smallest reductions (Fig. S1). On the other hand, a 30% reduction in biogenic emissions leads to greater changes in HCHO concentrations compared to a 30% reduction in anthropogenic emissions, with regional mean decreases of 8.2-19% (0.1-1.1 ppb). Surface CO concentrations also decrease by 1.4-6.2% (1.3-10 ppb), indicating similar ranges of sensitivity to biogenic and anthropogenic emissions. The most substantial reductions in HCHO and CO occur in the

eastern CONUS, where the spatial pattern aligns most closely with biogenic isoprene emissions, which are significantly higher than those of other biogenic VOC species and thus have the largest impact (Fig. S3).

As anticipated from the updated gas-phase chemistry for isoprene and terpenes outlined in Schwantes et al. (2020), switching to the MOZART-TS2 chemical mechanism increases surface HCHO and CO concentrations across the CONUS by 3.9-12% (0.1-1.0 ppb) and 0.4-3.5% (0.4-5.7 ppb), respectively. O₃ changes are small but exhibit greater spatial heterogeneity than HCHO and CO, with slight increases in the Midwest, Southwest, and Northeast by 0.8-1.7% on average and decreases on the West Coast, Mountain, and Southeast by 0.5-1.7%, all under 0.8 ppb.

Text S2. Sensitivity to Nudging Strength

Nudging is a modeling technique that involves applying an artificial Newtonian relaxation term based on the difference between the model reference state and meteorological re-analysis data, aiming to improve the agreement between simulated and actual states (Jiali Li et al., 2022; Otte, 2008). Stronger nudging of temperature and winds aims to closely replicate real-world meteorological conditions, thereby reducing meteorological bias relative to observations in the model (Davis et al., 2022; Gaubert et al., 2020; Schwantes et al., 2022). However, overly strong nudging can induce artificial mixing of atmospheric tracers, particularly across sharp gradients like those at the tropopause (van Noije et al., 2004). Concerns persist that specified dynamics schemes with nudging may inaccurately represent circulation trends and introduce tracer transport errors (Davis et al., 2022). We thus evaluate the impact of nudging strength by comparing 12-hour and 6-hour relaxation times applied to 'T' (air temperature), 'U' (zonal wind velocity), and 'V' (meridional wind velocity) through two additional simulations (*CAMS_6HrNudge_chemTS1* and *CAMS_6HrNudge_chemTS2*; Table S1) that replicate the BASE and CAMS_chemTS2 setups but use a shorter 6-hour relaxation time (stronger nudging strength).

When comparing simulations using the same nudging strengths with MOZART-TS2 versus MOZART-TS1, we find almost identical responses in the nudged variables T, U, V, and air pollutant concentrations as expected (Fig. S3). Despite differences attributed to weather noise, the discrepancies between the changes in surface conditions with 12-hour

and 6-hour nudging remain minimal, typically less than 0.01% for nudged variables and less than 1 ppb for surface O₃ and NO₂ and are largely driven by meteorological factors such as cloud cover and photolysis rates (see Schwantes et al. 2022 for more on nudging and specified dynamics relaxation times). Notably, the impact of this weather noise is not homogeneous, resulting in greater differences in O₃ than NO₂, and particularly pronounced in the Midwest compared to other regions.

We find that the differences resulting from nudging when two different relaxation time scales are used exceed differences attributed to switching chemical mechanisms when both perturbations use the same nudging strength (Fig. S3). Fig. S3 shows disparities between the MOZART-TS1 simulations using 6-hour and 12-hour nudging (BASE) are notably larger and exhibit significant regional variation, even for the nudged variables. Specifically, regional mean temperature changes range from -0.5 K in the Midwest to +0.2 K in the West Coast and Southeast. Changes in zonal (U) and meridional (V) wind velocities are less than 0.3 m/s. Additionally, changes in surface NO₂ concentrations are within 0.05 ppb, whereas surface O₃ shows more pronounced responses, particularly in the Southeast, where changes peak at 1.5 ppb while remaining under 0.8 ppb in other regions.

We emphasize that changes in concentrations due solely to the nudging configuration are non-negligible, and thus sensitivity tests should be conducted with a consistent and appropriately selected relaxation time. We adopt a consistent 12-hour relaxation time in our MUSICA_{v0} sensitivity simulations (Table 1) to ensure that differences among simulations reflect the intended perturbations rather than noise arising from differences in the nudging configuration.

Text S3. NEI Processing Approach

We first use the WRF Preprocessing System (WPS), developed for the Weather Research and Forecasting (WRF) model, to create a regular latitude/longitude grid at 0.1° × 0.1° over the contiguous United States (CONUS). Next, we employ the `epa_anthro_emis` pre-processor, developed by NCAR as one of the tools for the Weather Research and Forecasting model coupled with Chemistry (WRF-Chem), to map the NEI 2017 version 2 emissions onto this 0.1° × 0.1° grid. The processor takes Community Multiscale Air Quality (CMAQ)-ready day-specific hourly emission files and maps them onto a WRF domain. The NEI 2017 version 2 CMAQ files, originally provided by the U.S. EPA, are at a 12 km × 12 km

resolution. Detailed documentation of these tools can be found at <https://www2.acom.ucar.edu/wrf-chem/wrf-chem-tools-community>.

Text S4. Reducing Anthropogenic NO_x and VOC Emissions under NEI_monthly

We conduct two additional one-month sensitivity simulations under the NEI_monthly case to further examine changes in O₃ and its precursors and investigate the photochemical regime of O₃ production using NEI emissions. One simulation applies a 30% reduction in anthropogenic NO emissions (*NEI_monthly_m30anthroNO*), while the other applies a 30% reduction in anthropogenic VOC emissions (*NEI_monthly_m30anthroVOC*) (Table 1). The VOC species considered in the latter simulation include acetylene, ethene, ethanol, ethane, propene, propane, methanol, acetone, methyl ethyl ketone (MEK), benzene, toluene, monoterpenes, isoprene, formaldehyde, other aldehydes, alkenes, and alkynes. These simulations specifically provide a comparison to the more nuanced changes resulting from imposing different temporal resolution of anthropogenic emissions in *NEI_hourly*, *NEI_hourly_NO*, and *NEI_daily_NO* simulations.

A 30% reduction in anthropogenic NO emissions results in regional average decreases in surface concentrations of NO (13-21%, 0.02-0.04 ppb), NO₂ (14-21%, 0.1-0.3 ppb), HCHO (2.8-4.5%, 0.1-0.2 ppb), and O₃ (4.7-8.0%, 1.9-2.9 ppb) across all regions (Fig. 3). Changes in VOC concentrations are minimal (generally less than a 5% increase), except for isoprene, which shows regional mean increases of 7-43% (0.1-0.4 ppb), with the largest changes in VOCs occurring in the Southwest and Southeast. This increase in isoprene is likely driven by reduced OH availability following NO emission reductions, which slows isoprene oxidation by limiting OH regeneration through the NO + HO₂ reaction. Additionally, lower O₃ levels reduce ozonolysis of isoprene and other VOCs, further contributing to isoprene accumulation.

A 30% reduction in anthropogenic VOC emissions results in regional average decreases in VOC species primarily from anthropogenic sources, such as benzene (7.7-21%, around 0.01 ppb). In contrast, HCHO and isoprene, which are largely dominated by biogenic sources, show minimal changes: HCHO decreases slightly (0.4-0.7%, 0.01-0.03 ppb), while isoprene exhibits small regional increases of less than 2% in the Northeast, Southwest, and Southeast, and less than 0.2% in other regions. Changes in NO, NO₂ and O₃ are all negligible (less than 0.5% or 0.01 ppb; not shown).

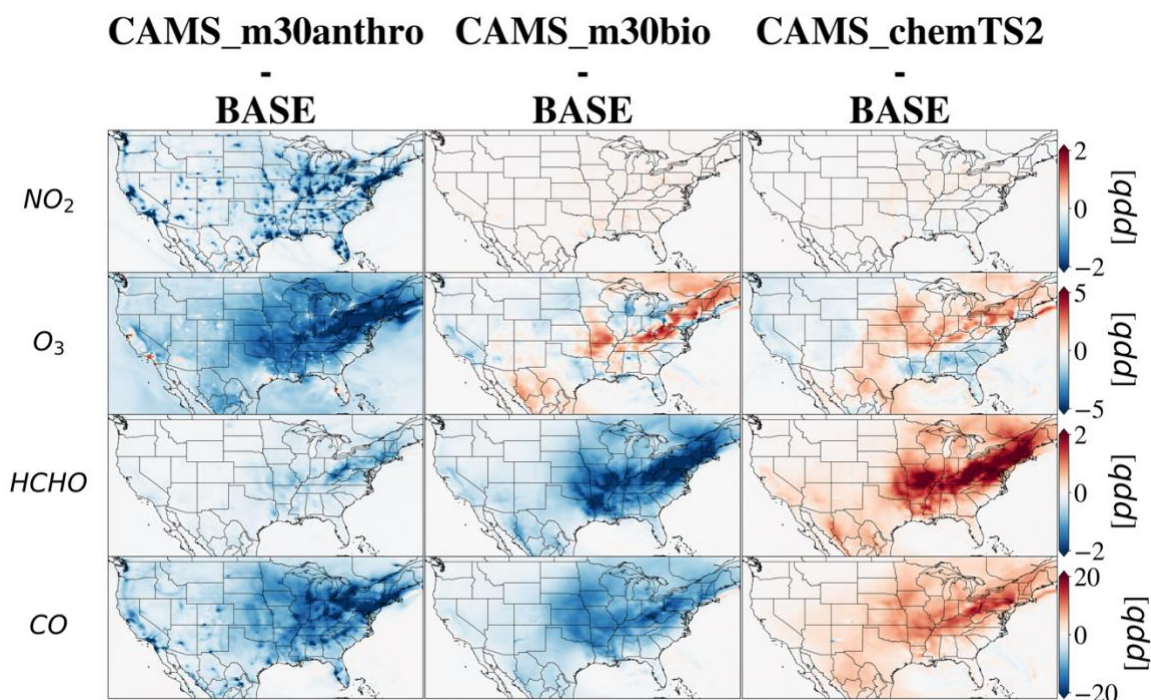
The spatial variations in O₃ concentrations in response to changes in anthropogenic NO or VOC emissions reflect distinct photochemical conditions (Fig. 3). Metropolitan areas such as New York City (NY) and Los Angeles (CA), which have the highest initial NO emissions (Fig. S4) and show the largest NO₂ reductions under a 30% decrease in anthropogenic NO emissions (Fig. 3), imply NO_x-saturated regimes since O₃ increases when NO_x levels decrease and O₃ decreases with reductions in VOCs. Conversely, regions outside major cities appear more NO_x-sensitive, where O₃ decreases with reduced NO_x and remains relatively unchanged with VOC reductions. Overall, O₃ concentrations respond more strongly to a 30% reduction in NO emissions than to an equivalent reduction in anthropogenic VOC emissions.

Text S5. Evaluation of Surface SO₂ and PM_{2.5} Simulations

For the BASE simulation, we consistently find a high model bias in surface SO₂, ranging from 50% to 94% (0.9-11 ppb), with poor spatial correlation and high RMSE relative to observations. Surface PM_{2.5} estimates exhibit low biases of 15%-44% (1.0-2.4 µg/m³) in the Mountain, Midwest, and Southwest regions, while they are biased high by 27%-34% (3.2-5.1 µg/m³) in the West Coast, Northeast, and Southeast, with model-observation correlation coefficients varying between 0.15 and 0.75.

Switching to the NEI emissions decreases regional July averages for surface SO₂ and PM_{2.5} by 250-830% (0.3-1.7 ppb) and 2.2-11% (0.3-0.8 µg/m³), respectively. Nevertheless, comparisons with SLAMS observations reveal inconsistent model performance for SO₂ and PM_{2.5}, with only some regions improving (Table S3). For SO₂, biases shift from overestimates to underestimates in all regions except the Southwest, with MBE and RMSE values moving closer to zero. However, r_s decreases in the Southwest, Northeast, and Southeast. Spatial correlation for PM_{2.5} improves solely in the Southeast but weakens elsewhere. After incorporating hourly-resolved emissions, we find a regional average increase in monthly mean surface SO₂, ranging from 5-72% (less than 0.1 ppb) and r_s remains poor. For surface PM_{2.5}, the differences in regional average monthly mean concentrations between NEI_hourly and NEI_monthly generally increase across the CONUS, ranging from 1.3-11% (0.2-0.7 µg/m³) (Fig. S2 and Table S3).

(a) Surface concentrations



(b) Tropospheric vertical column densities (VCD_{Trop})

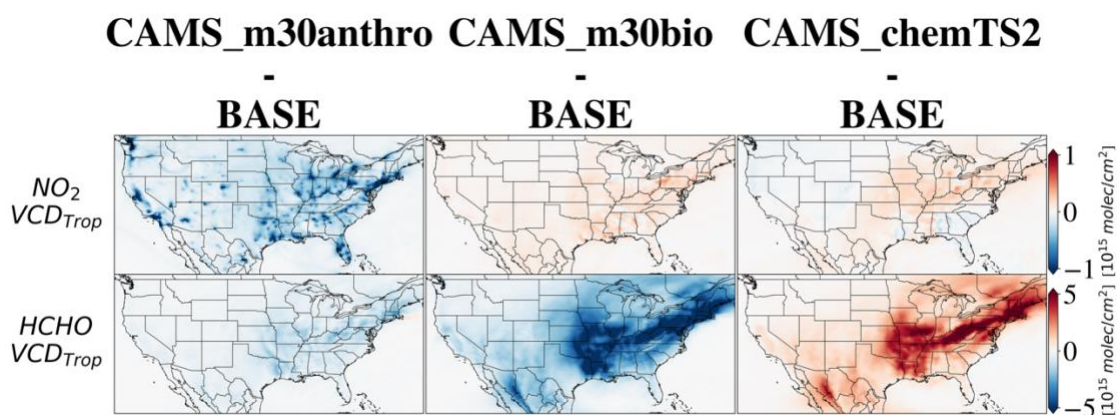


Fig. S1. Responses of selected trace gas species (rows: surface concentrations in panel a, column densities in panel b) to five-day perturbation simulations (July 1-5, 2018; see Table S1), shown as differences in five-day means relative to the BASE case. Consistent color-bar ranges are used for each variable. See Fig. S2 for differences in surface SO_2 and $PM_{2.5}$.

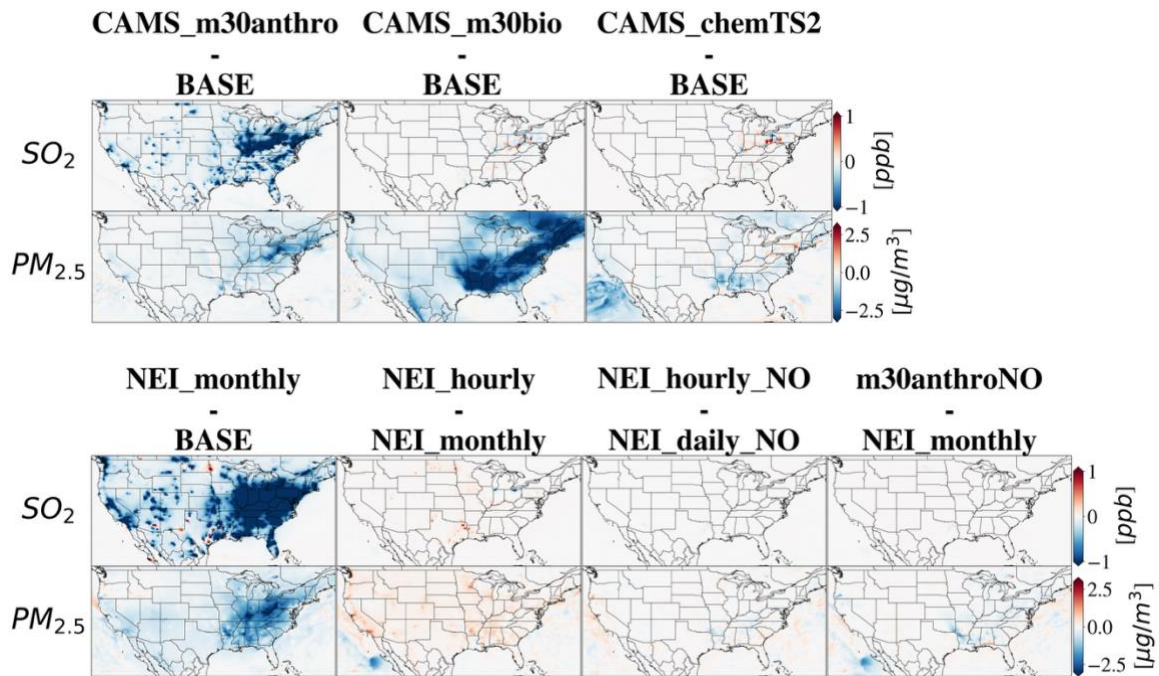


Fig. S2. Same as Fig. 3a and Fig. S1a, but for changes in surface concentrations of SO_2 (first row) and $PM_{2.5}$ (second row).

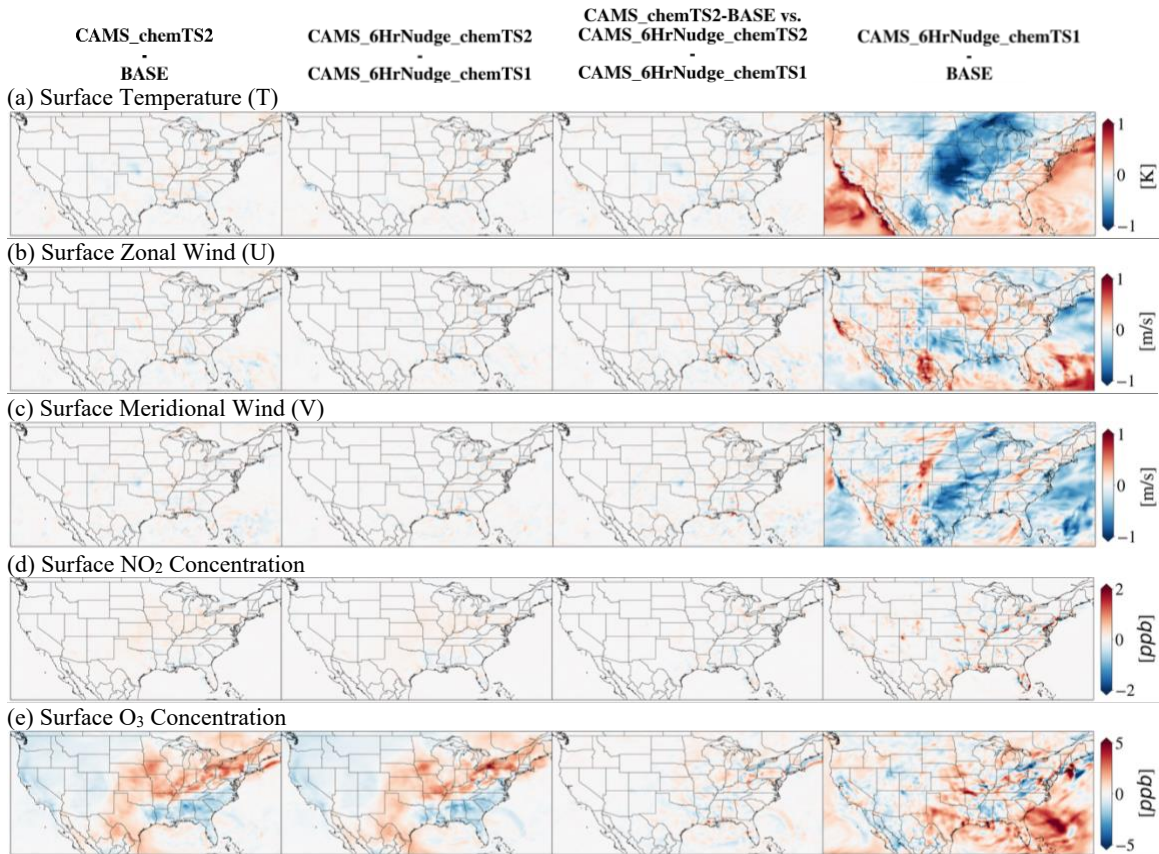
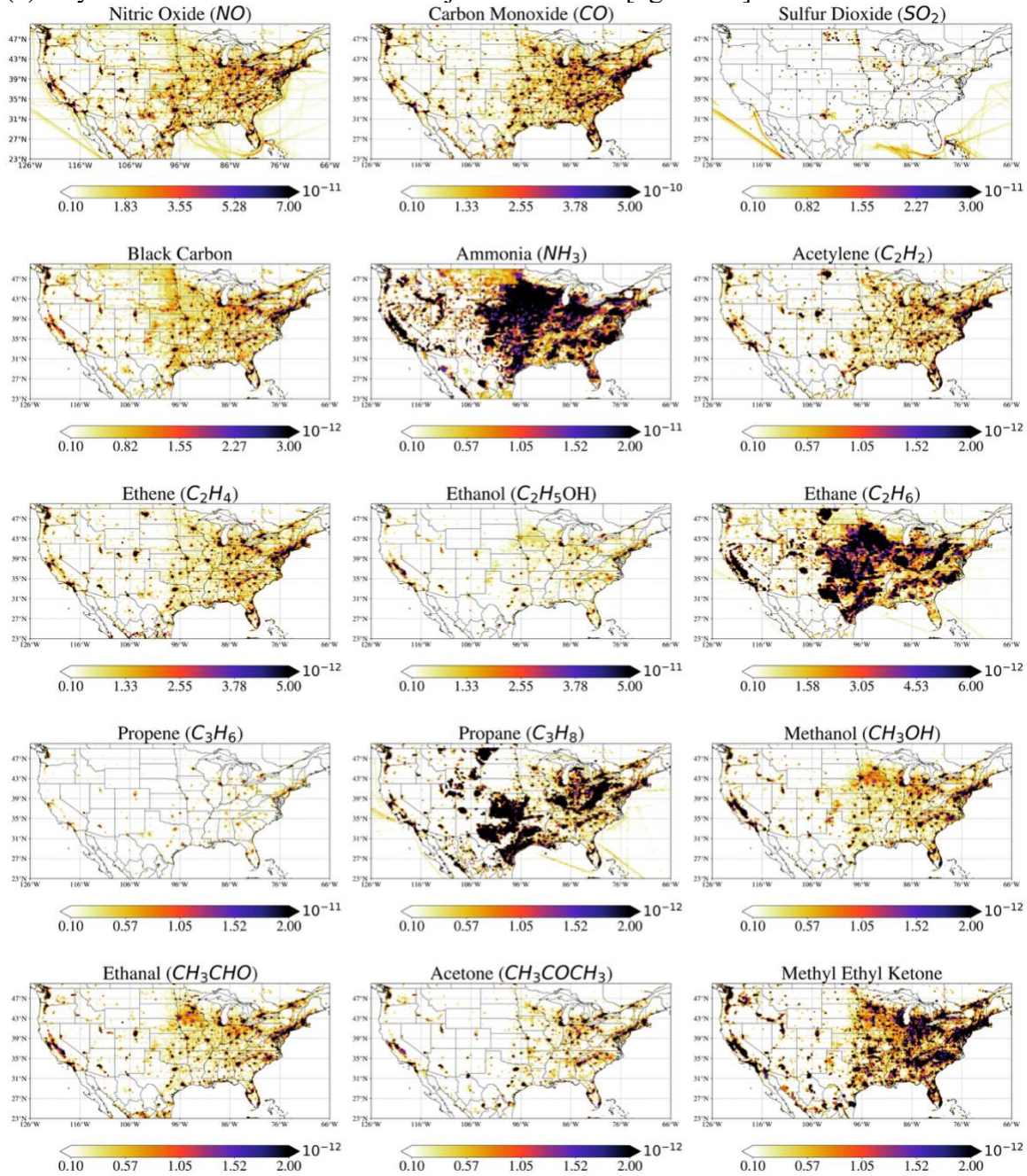
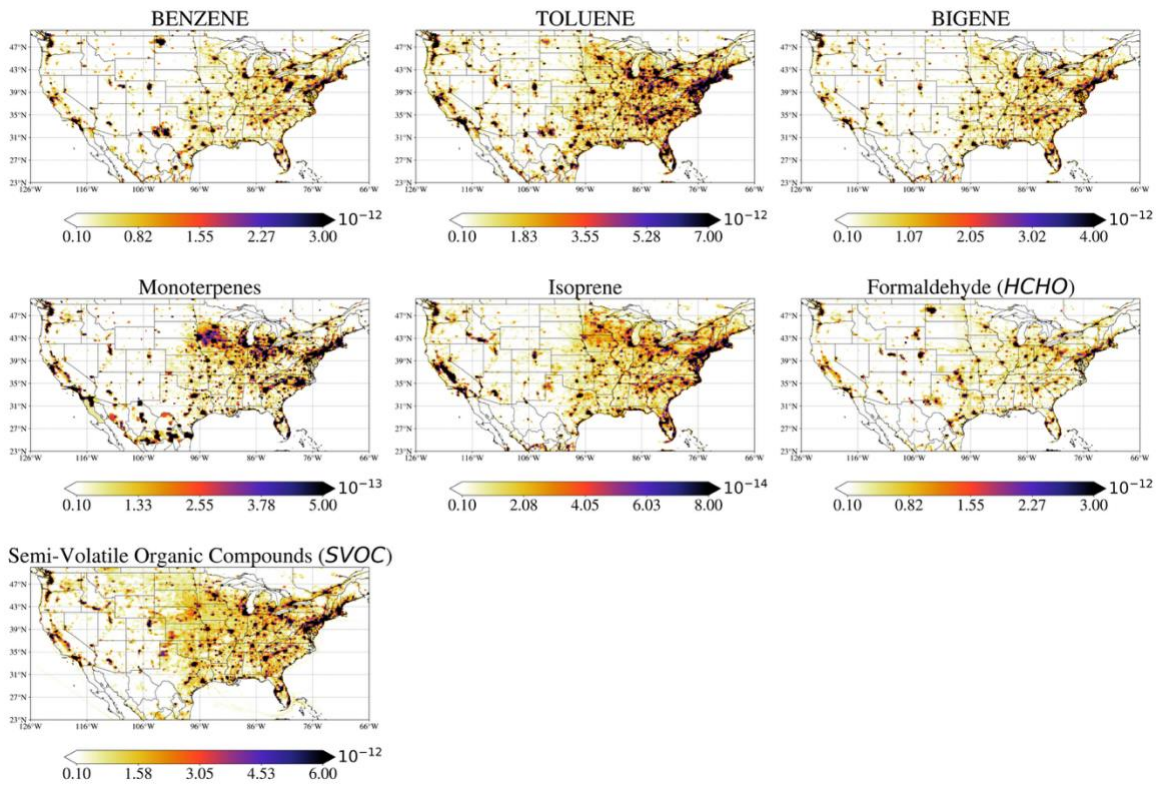


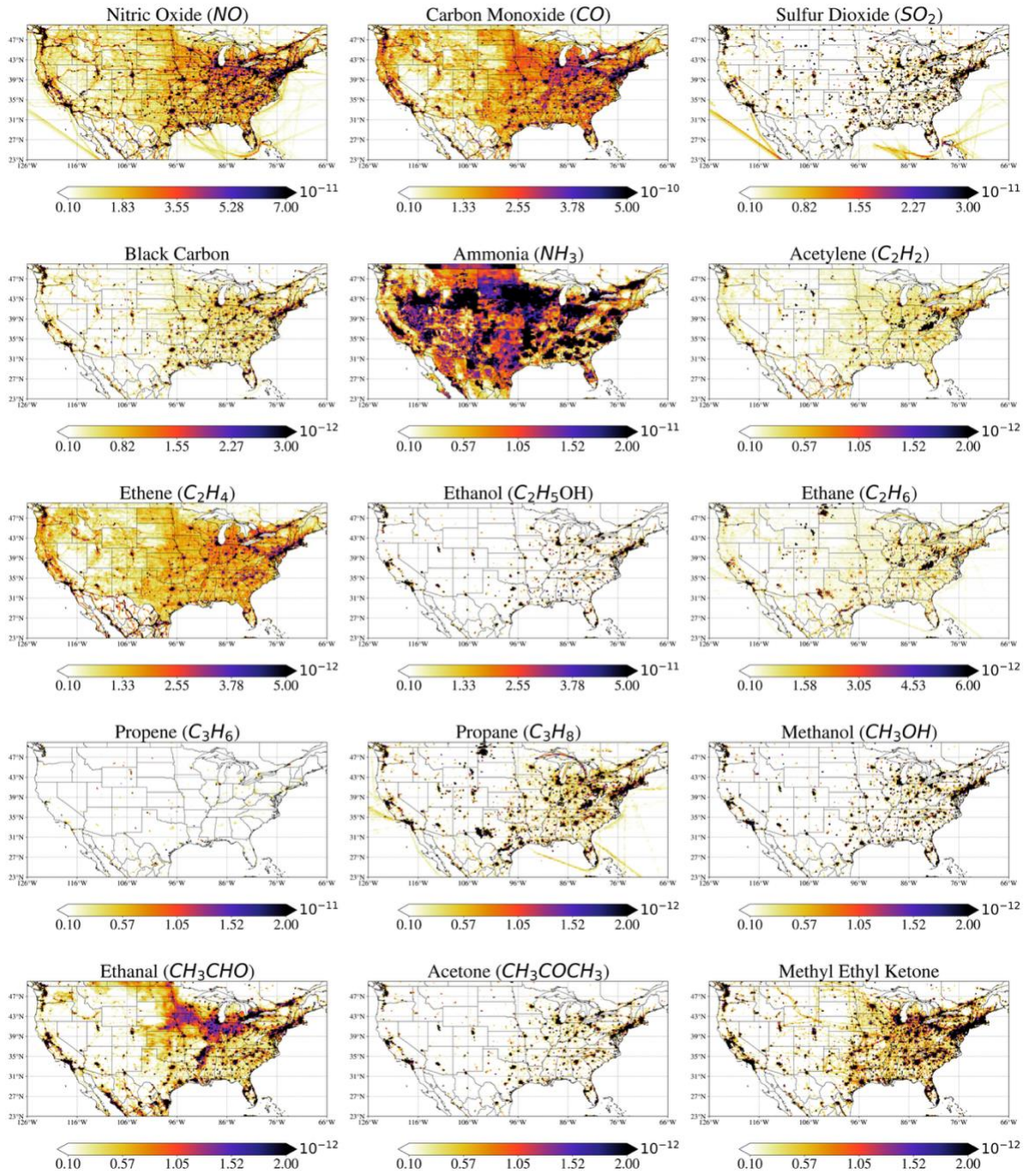
Fig. S3. Differences for surface T, U, V, NO₂ and O₃ concentrations across simulations using the MOZART-TS1 (BASE) and MOZART-TS2 chemical mechanisms with 12-hour (CAMS_chemTS2) and 6-hour nudging relaxation times (CAMS_6HrNudge_chemTS1 and CAMS_6HrNudge_chemTS2). Simulations using the same nudging strength produce similar meteorological conditions and trace gas concentrations, whereas changing the nudging strength can lead to substantial differences. The first two columns compare MOZART-TS1 versus MOZART-TS2 differences for each nudging option, while the third column contrasts these differences across different nudging options. The rightmost column contrasts the impacts of 6-hour nudging on simulations with the BASE 12-hour simulations.

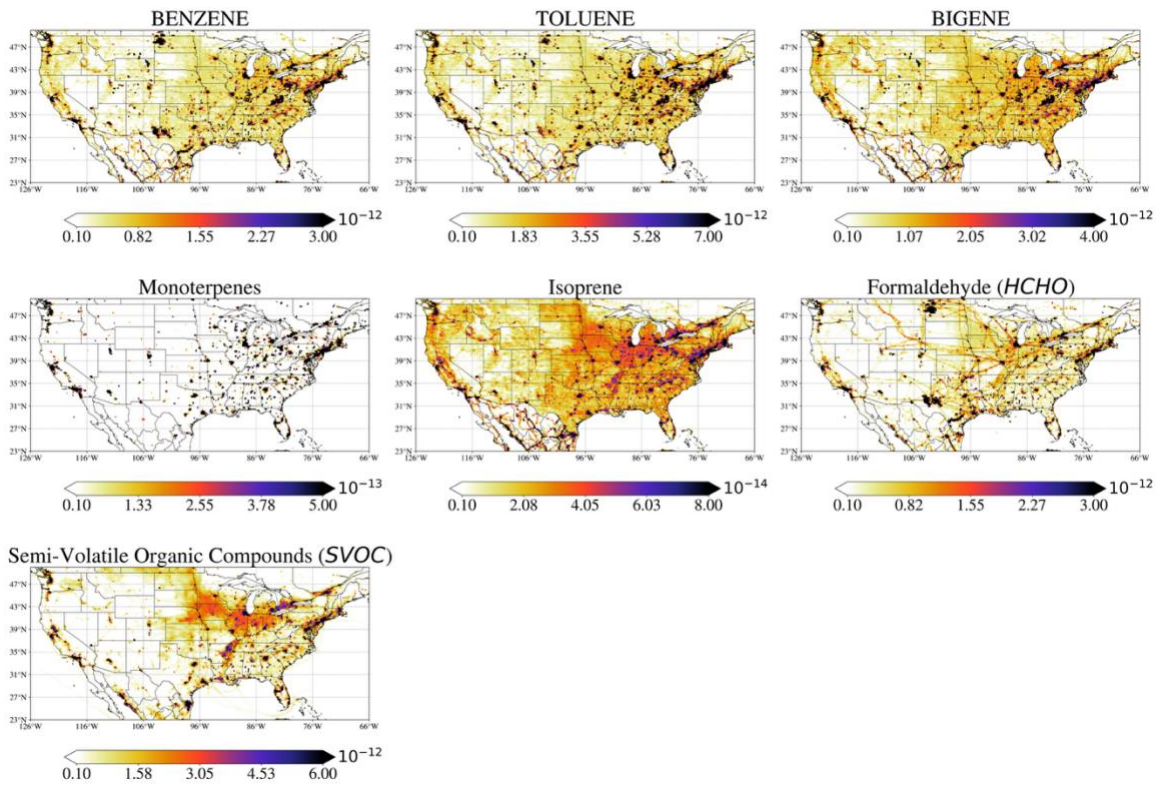
(a) July Mean NEI 2017 Emissions Adjusted for 2018 [$\text{kg m}^{-2} \text{s}^{-1}$]



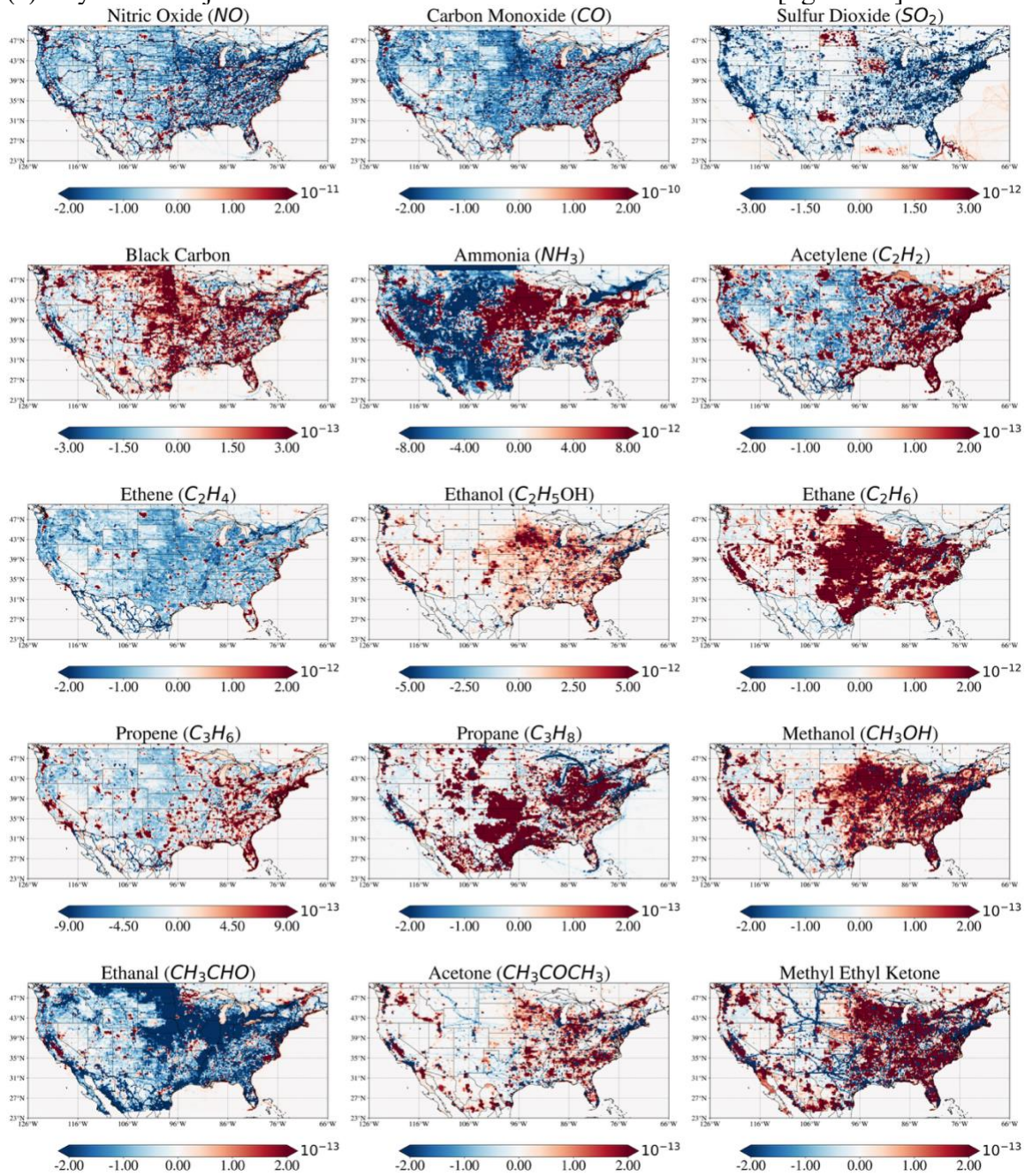


(b) July Mean CAMS-GLOB-ANT v5.1 Emissions [$\text{kg m}^{-2} \text{s}^{-1}$]





(c) July Mean Adjusted NEI Minus CAMS-GLOB-ANT Emissions [$\text{kg m}^{-2} \text{s}^{-1}$]



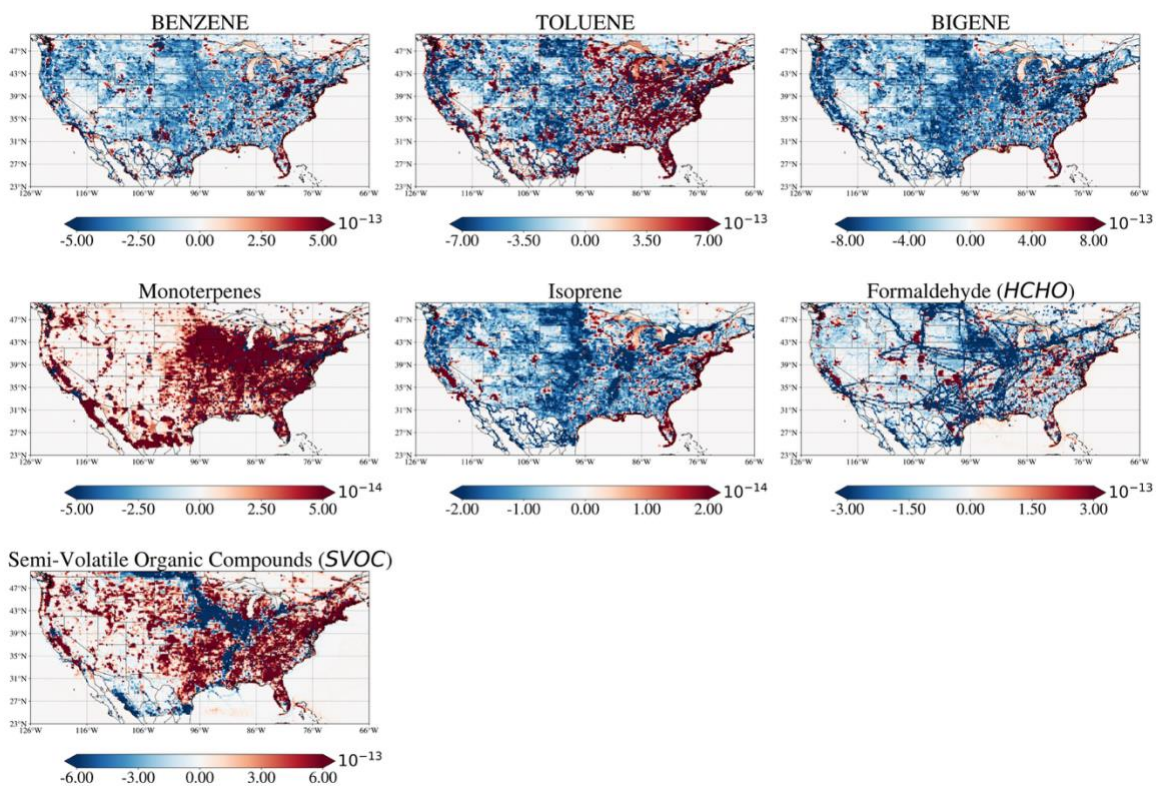


Fig. S4: Spatial distribution of July mean emissions from the adjusted 2017 U.S. National Emissions Inventory (NEI; panel a), Copernicus Atmosphere Monitoring Service (CAMS-GLOB-ANT v5.1; panel b), and their differences (panel c) for each species replaced with NEI emissions in the MUSICA_{v0} simulations over the contiguous United States (CONUS).

MEGAN Biogenic Emissions [$\text{kg m}^{-2} \text{s}^{-1}$]

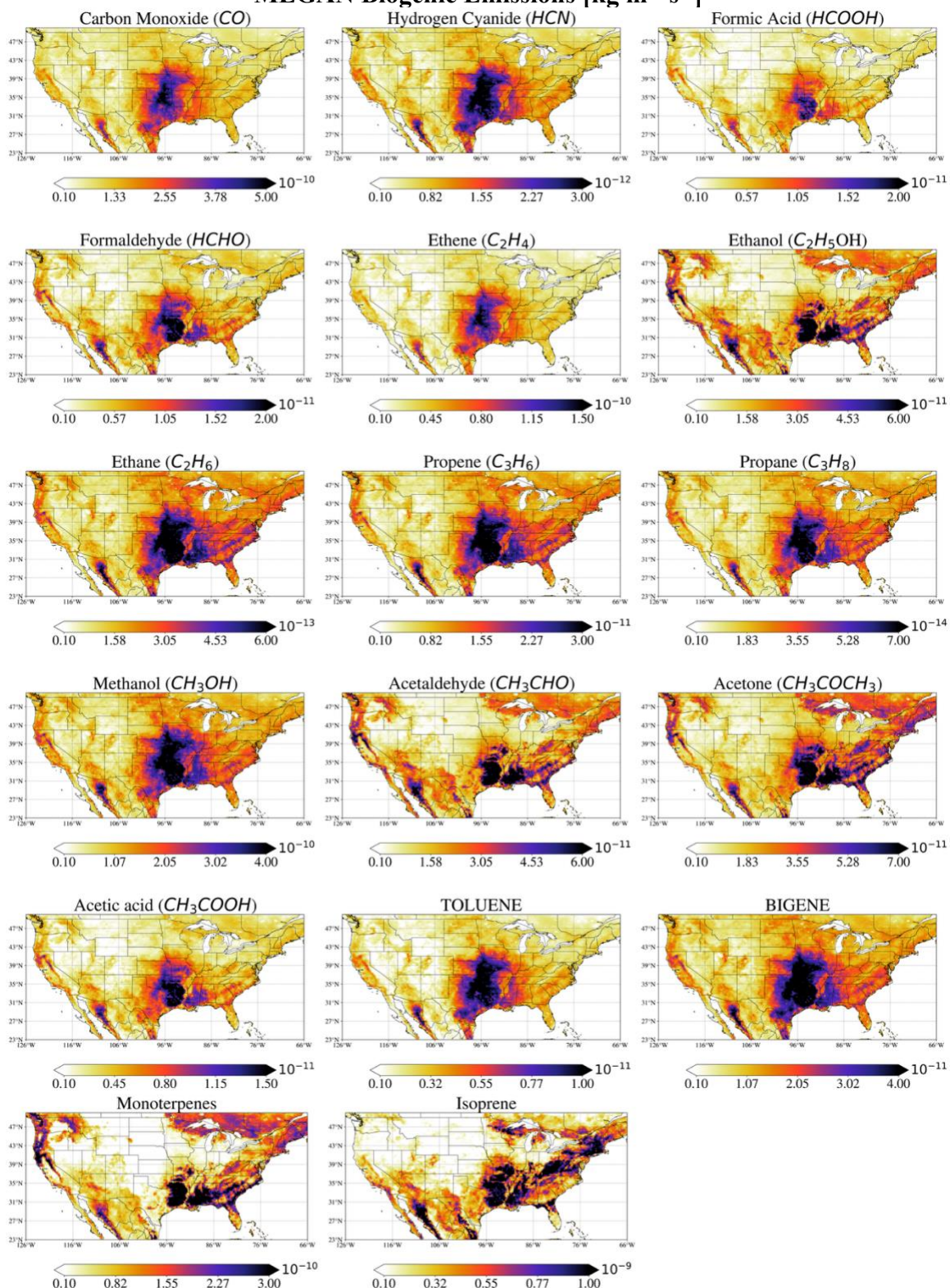
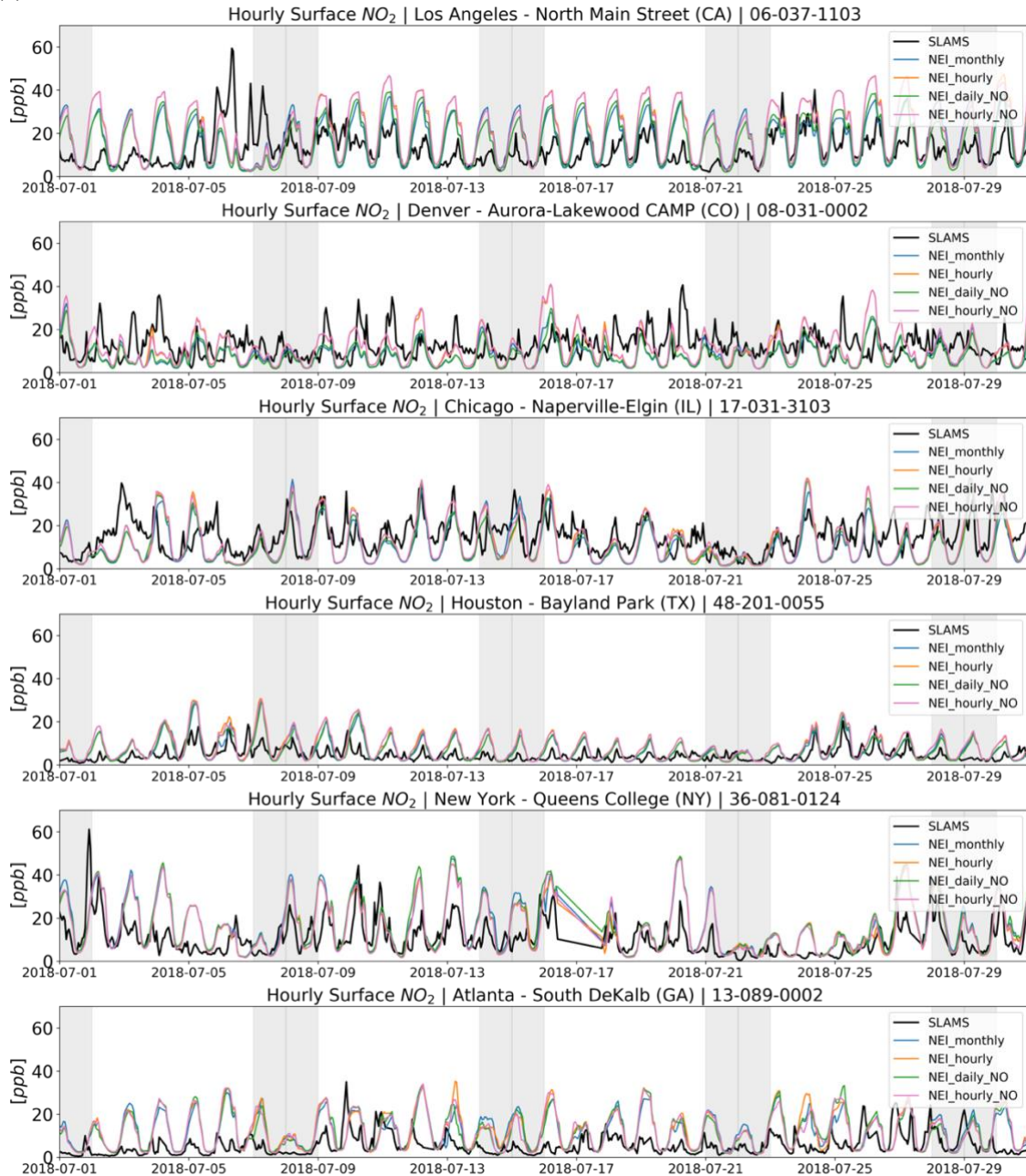


Fig. S5. The spatial distribution of biogenic emissions calculated online in the land component of CESM using the Model of Emissions of Gases and Aerosols from Nature

(MEGAN) version 2.1 in the NEI_monthly case simulation. Relative differences in any biogenic emission species across the NEI simulations remain below 10%, even in the grid cell with the largest change, which occurs primarily in the southern CONUS due to weather-induced variability that persists even with 12-hour nudging (not shown).

Observed versus Modeled Hourly Concentrations

(a) Surface NO₂



(b) Surface O₃

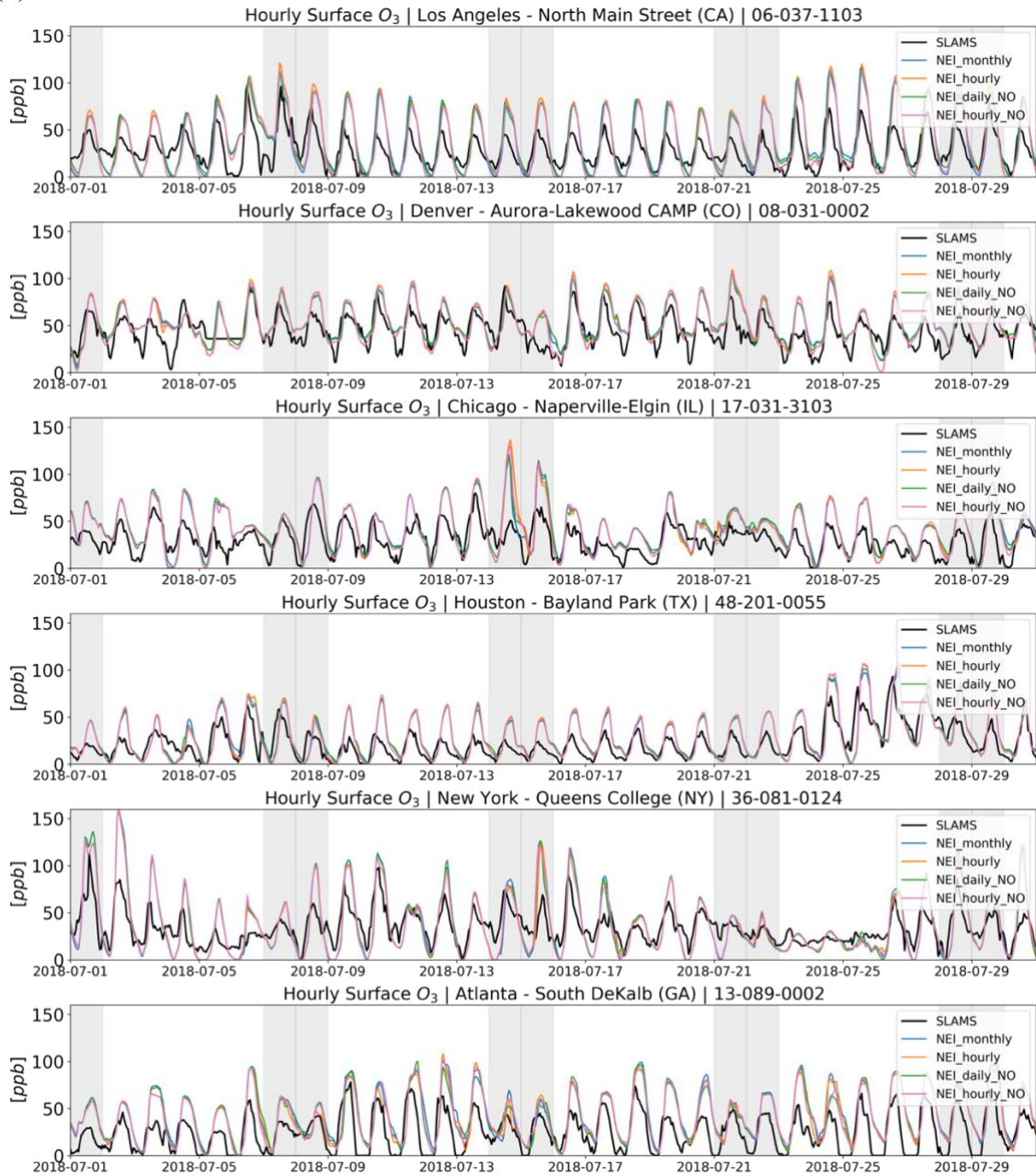
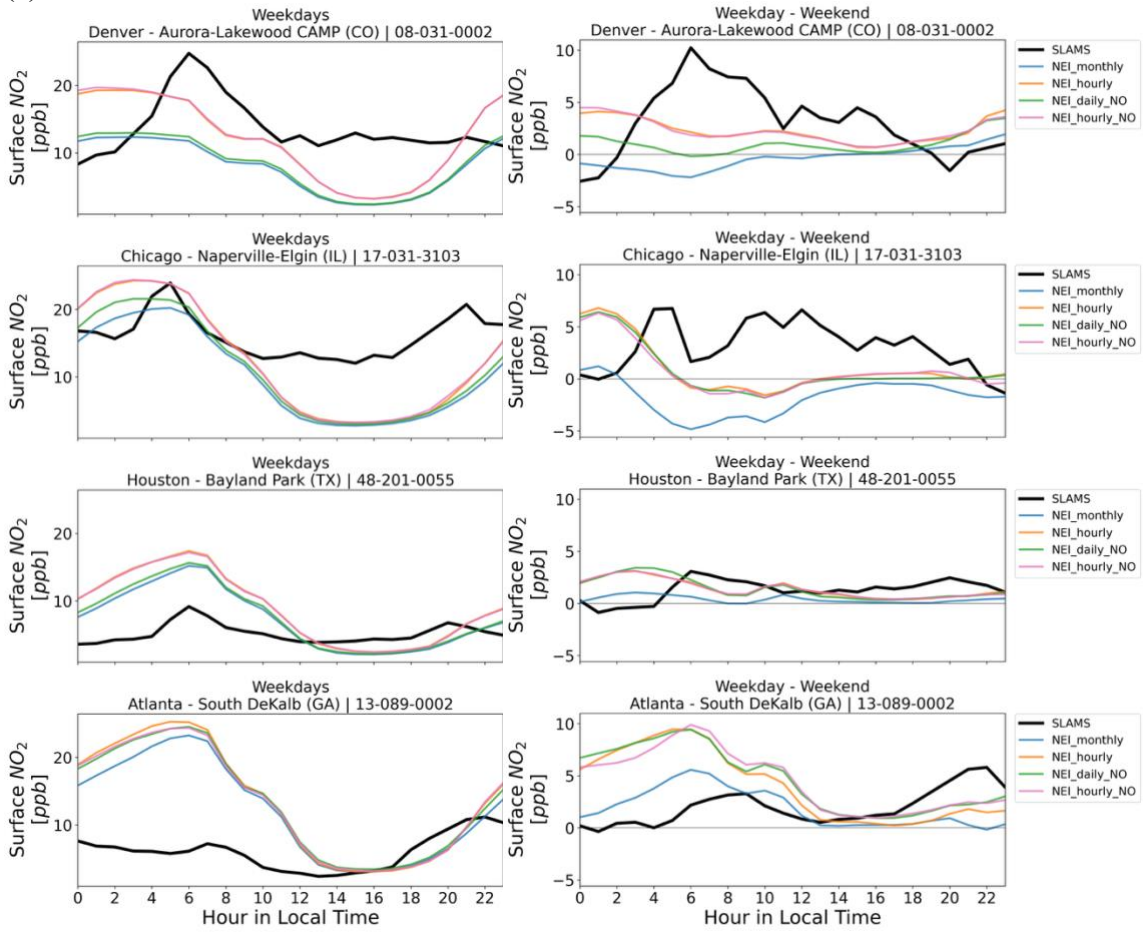


Fig. S6: Hourly variations in surface NO₂ (a) and O₃ (b) concentrations from observations and model simulations for July 2018 at six selected urban monitoring stations (Table S5). Observations from SLAMS are in black. Model simulations are shown in four scenarios: NEI_monthly (blue), NEI_hourly (orange), NEI_daily_NO (green), and NEI_hourly_NO (pink). Near-surface simulations are approximated at the nearest pixel to each monitoring station. Weekend days (Saturdays and Sundays) are marked in gray.

(a) Surface NO₂



(b) Surface O₃

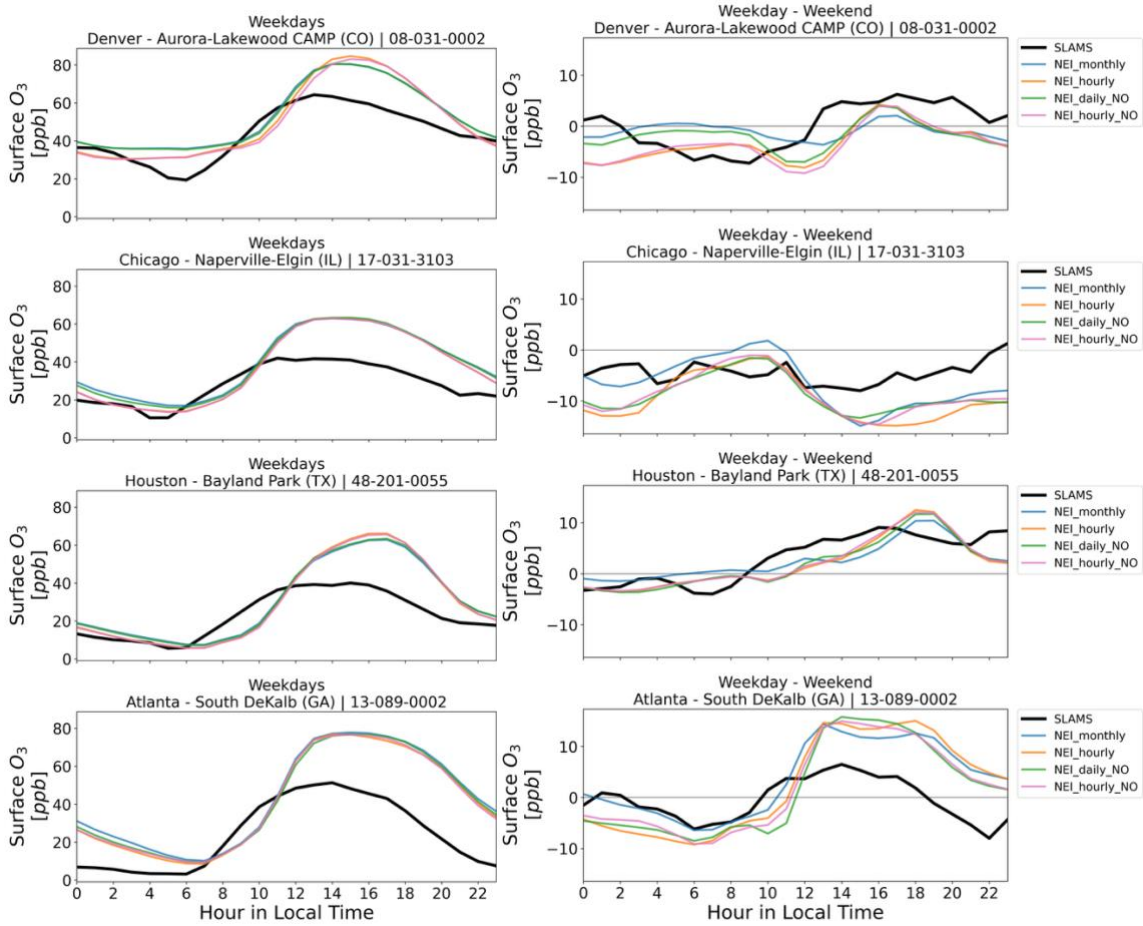
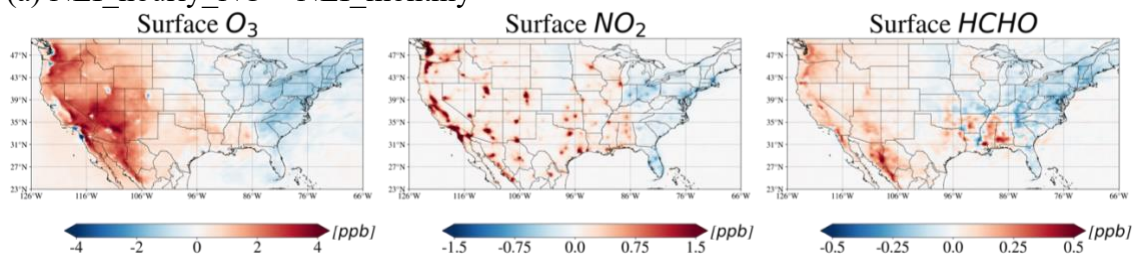


Fig. S7: Simulated hourly diel cycles of July mean concentrations on weekdays only (left column) and weekday minus weekend differences (right column) for four one-month simulations with perturbations in the temporal resolution of anthropogenic emissions (Table 1), shown by different colored lines, for NO₂ (panel a) and O₃ (panel b).

(a) NEI_hourly_NO – NEI_monthly



(b) NEI_daily_NO – NEI_monthly

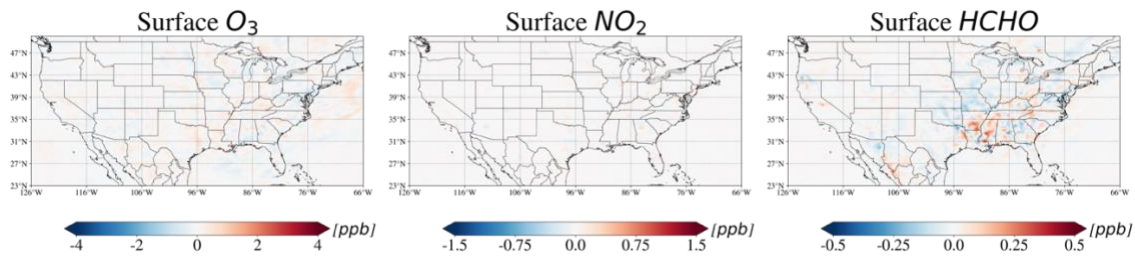


Fig. S8: July mean differences in simulated surface concentrations of O_3 , NO_2 , and $HCHO$ between (a) NEI_hourly_NO and NEI_monthly, and (b) NEI_daily_NO and NEI_monthly. These comparisons complement Fig. 3, highlighting that the spatial differences are primarily driven by the inclusion of hourly variability in NO emissions.

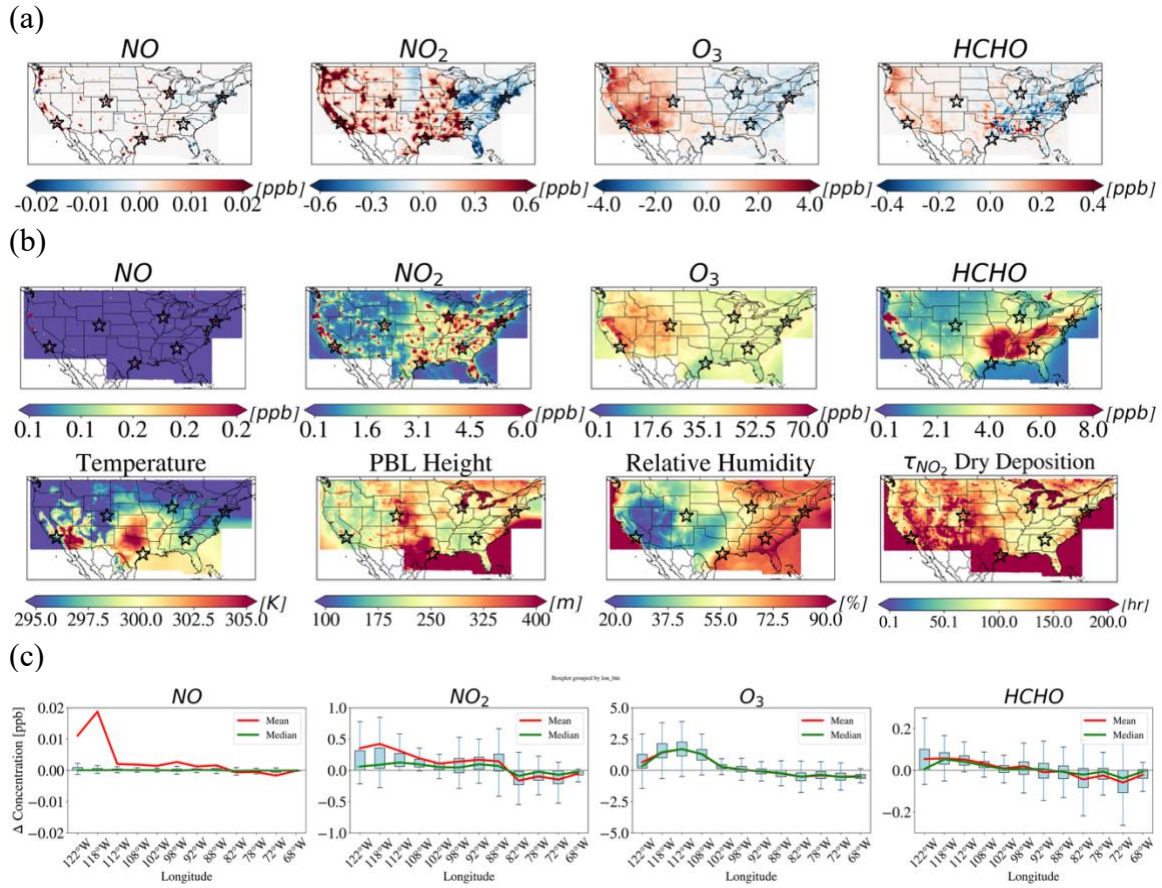


Fig. S9: Same as Fig. 5, but for nighttime (11 p.m.-5 a.m. local time) monthly mean differences and values.

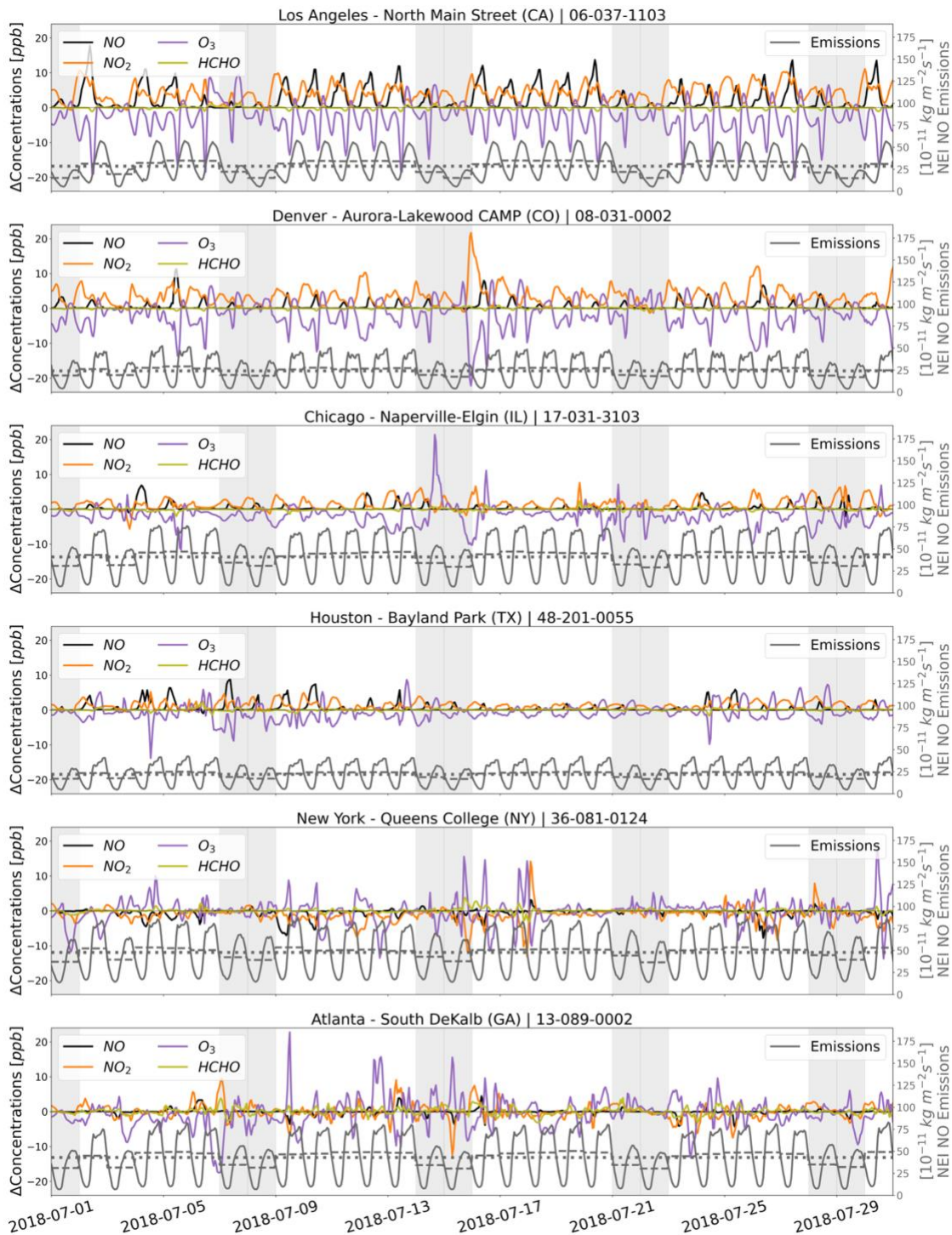
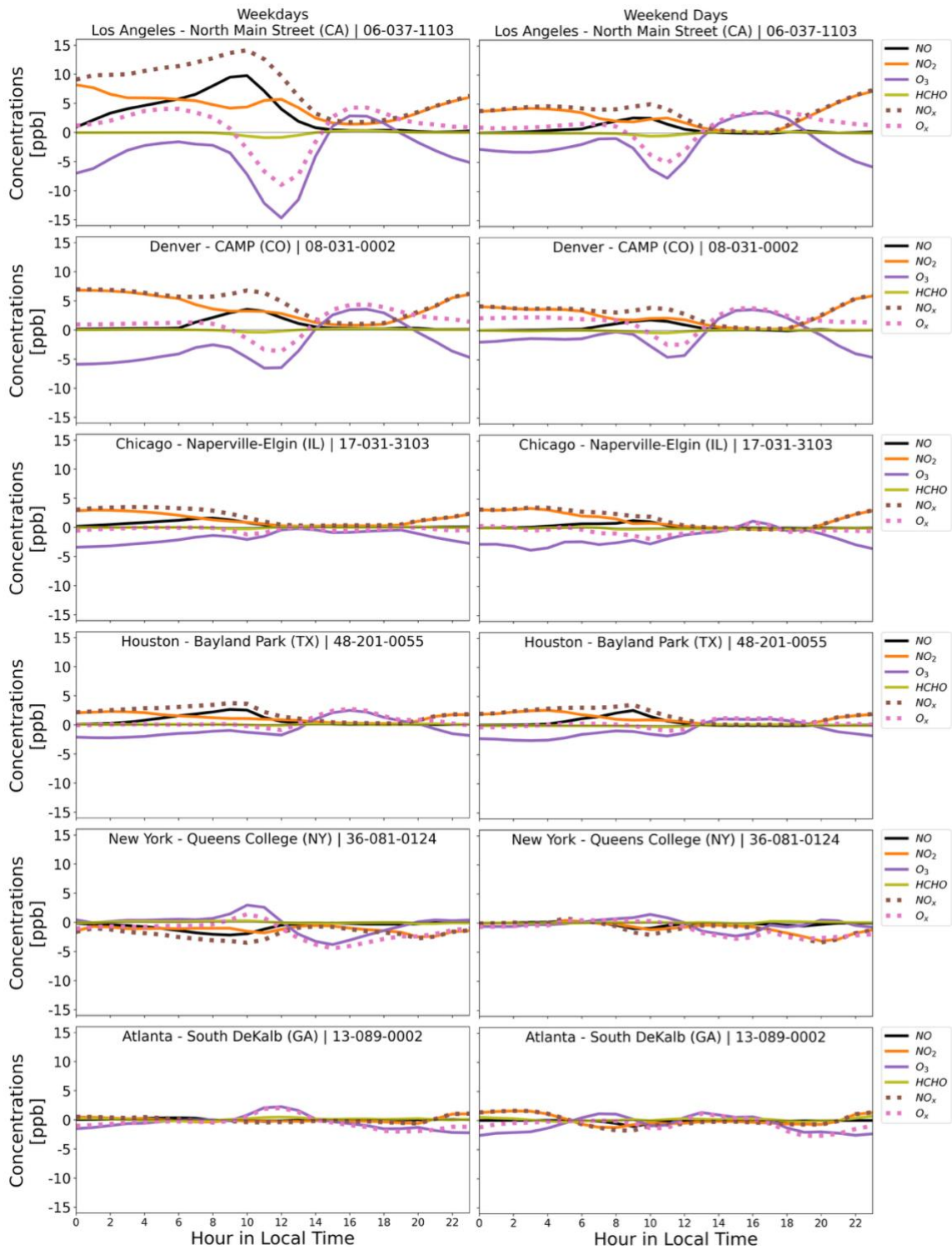


Fig. S10: Same as Fig. 6a but extended to include surface concentrations of NO₂ (orange) O₃ (purple), and HCHO (olive), in addition to NO (black), across six cities. NEI NO emissions are shown as monthly means (dotted), daily means (dashed), and hourly values (solid gray). All data are in local time; weekends are shaded in gray.

(a)



(b)

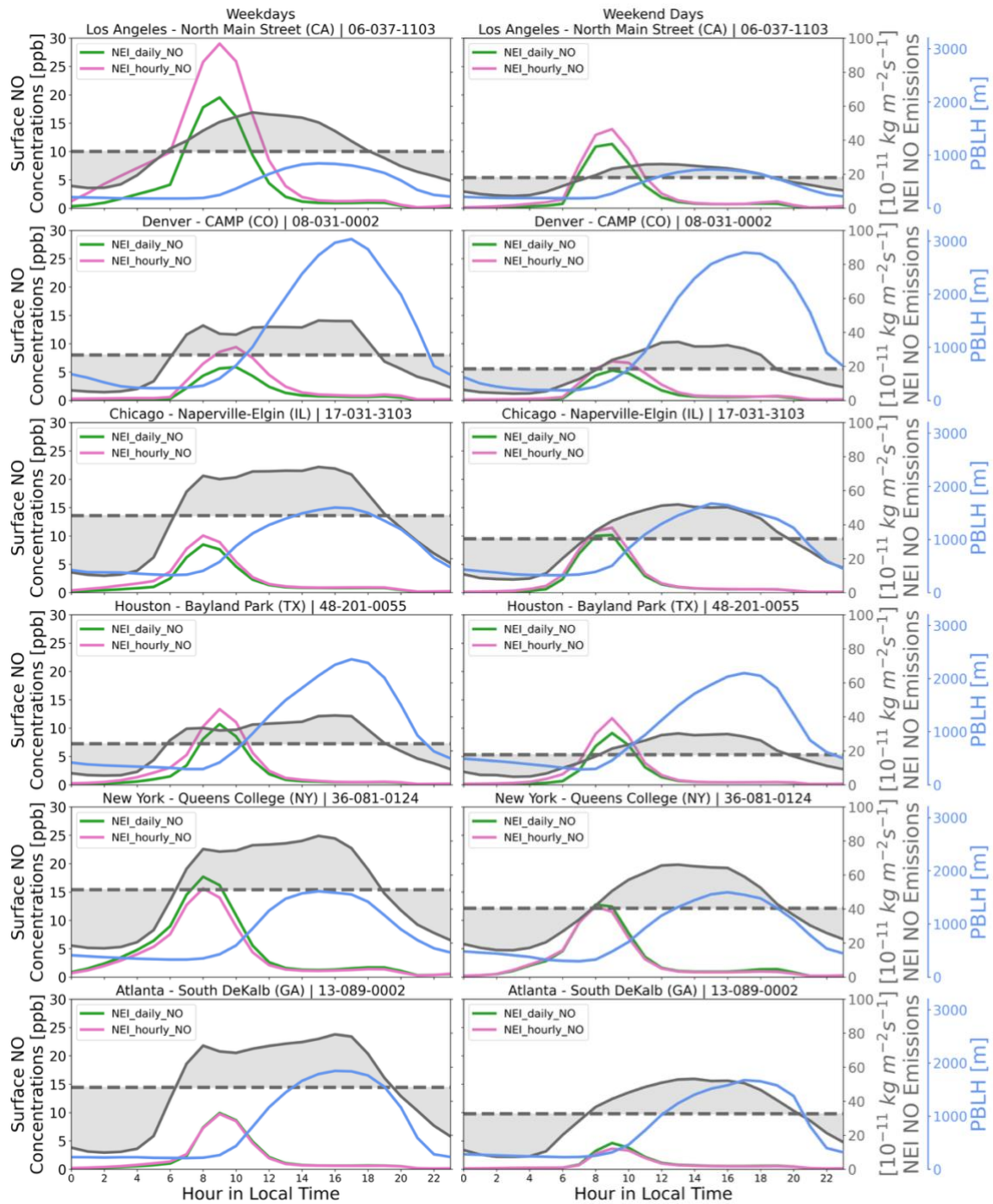


Fig. S11: Same analysis as Fig. 6 but extended to all sites and including July 2018 weekend-day averages (left column) in addition to weekday (right column). Panel (a) corresponds to Fig. 6b and shows hourly surface concentrations of NO, NO₂, O₃, and HCHO; panel (b) corresponds to Fig. 6c and shows hourly NO concentrations from NEI_daily_NO and NEI_hourly_NO, plotted with NO emissions and planetary boundary layer height (PBLH).

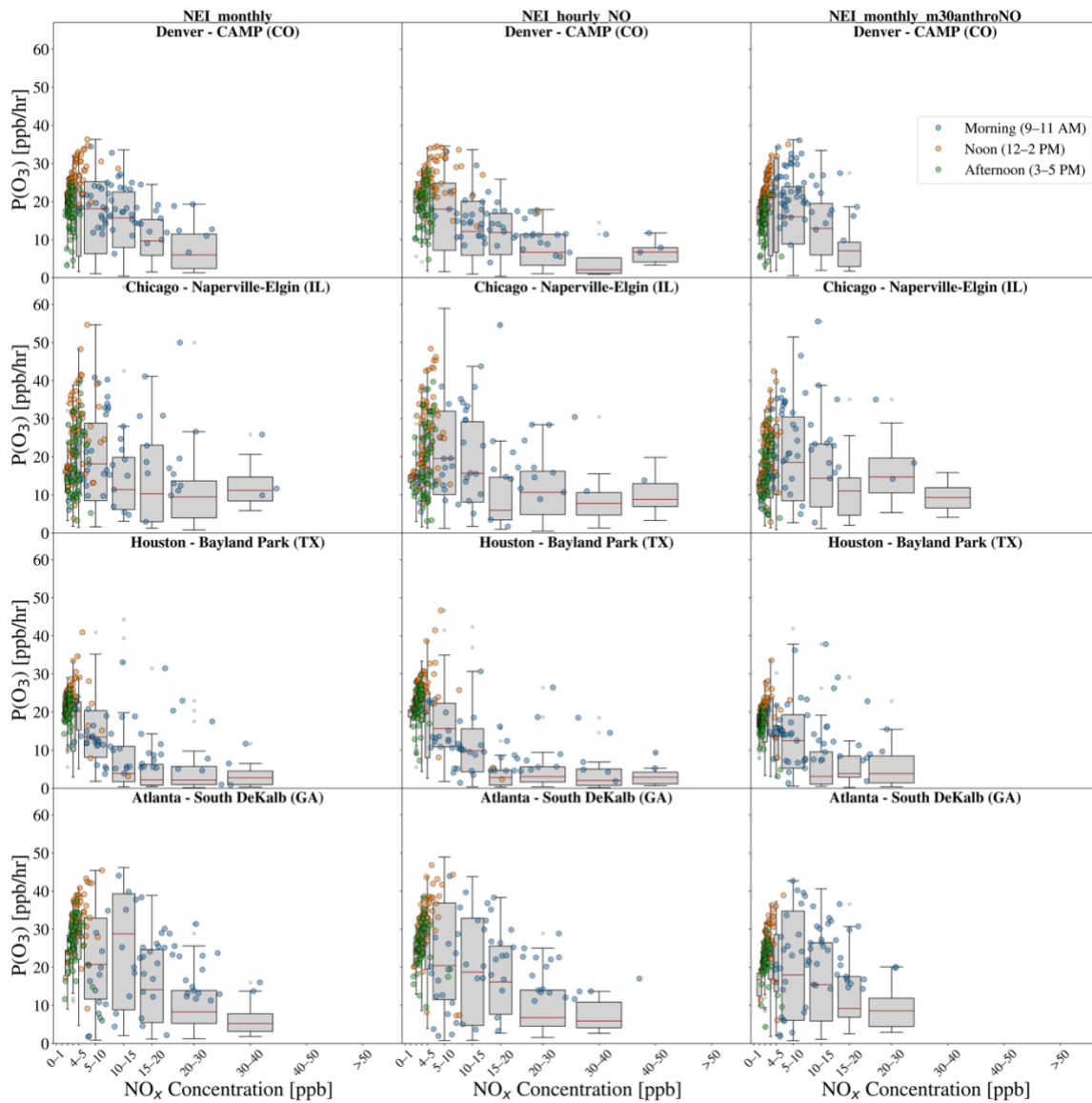


Fig. S12: Same as Fig. 7, but for sites in Denver (CO), Chicago (IL), Houston (TX), and Atlanta (GA).

Table S1. Five-day sensitivity simulations (July 1-5, 2018) used to test model responses to changes in anthropogenic and biogenic emissions and to an alternative chemical mechanism, relative to the BASE case.

Simulation ID	Chemical Mechanism	Nudging Strength	Simulation Period	Emissions Perturbation
CAMS_m30anthro	MOZART-TS1	12-hour	July 1-5, 2018	-30% total anthropogenic emissions
CAMS_m30bio	MOZART-TS1			-30% total biogenic emissions
CAMS_chemTS2	MOZART-TS2	No		
CAMS_6HrNudge_chemTS1	MOZART-TS1	6-hour		No
CAMS_6HrNudge_chemTS2	MOZART-TS2		No	

Table S2. Comparison of July mean modeled surface concentrations of NO₂, O₃, and CO with SLAMS observations from all available monitoring sites, and of tropospheric vertical column densities (VCD_{Trop}) of NO₂ and HCHO, and total vertical column densities (VCD_{Total}) of CO with TROPOMI. Results are shown for the BASE, NEI_monthly, and NEI_hourly cases (details in Table 1). Model performance is evaluated using Spearman's rank correlation coefficient (r_s), mean bias error (MBE), and root mean square error (RMSE), calculated separately for each region. These statistics correspond to the r_s and MBE values shown in Fig. 2, while this table provides a more comprehensive summary including RMSE. For MBE and RMSE, both the absolute values and the relative differences (in parentheses) are reported in this table. Surface SO₂ and PM_{2.5} are included in Table S3.

	Region /Simulation ID	West Coast	Mountain	Midwest	Southwest	Northeast	Southeast
Surface NO ₂ [ppb]							
r_s	BASE	0.57	0.75	0.75	0.44	0.58	0.72
	NEI_monthly	0.65	0.76	0.78	0.57	0.65	0.73
	NEI_hourly	0.66	0.78	0.79	0.57	0.64	0.71
MBE (%)	BASE	4.73 (67 %)	-0.64 (-15 %)	1.63 (32 %)	3.22 (60 %)	4.05 (61 %)	1.77 (27 %)
	NEI_monthly	-0.93 (-13 %)	-1.46 (-35 %)	-0.69 (-13 %)	-0.48 (-9.0 %)	-0.79 (-12 %)	-0.43 (-6.7 %)
	NEI_hourly	1.03 (15 %)	-0.51 (-12 %)	-0.35 (-6.9 %)	0.36 (6.8 %)	-1.33 (-20 %)	-0.80 (-12 %)
RMSE (%)	BASE	8.81 (124 %)	3.11 (74 %)	3.06 (60 %)	5.33 (100 %)	7.08 (106 %)	3.96 (61 %)

	NEI_monthly	4.85 (68 %)	3.27 (78 %)	2.48 (48 %)	3.02 (57 %)	3.96 (59 %)	3.40 (53 %)
	NEI_hourly	5.35 (75 %)	3.03 (72 %)	2.48 (48 %)	3.17 (59 %)	4.07 (61 %)	3.55 (55 %)
Surface O ₃ [ppb]							
r_s	BASE	0.79	0.57	0.36	0.71	0.15	0.48
	NEI_monthly	0.81	0.56	0.47	0.81	0.52	0.50
	NEI_hourly	0.80	0.54	0.46	0.81	0.52	0.51
MBE (%)	BASE	9.34 (24 %)	6.04 (13 %)	13 (39 %)	12 (38 %)	9.73 (29 %)	11 (40 %)
	NEI_monthly	7.95 (21 %)	1.37 (2.9 %)	6.92 (21 %)	6.59 (21 %)	4.38 (13 %)	7.75 (27 %)
	NEI_hourly	9.08 (24 %)	2.65 (5.6 %)	6.55 (19 %)	6.71 (22 %)	3.12 (9.1 %)	6.92 (24 %)
RMSE (%)	BASE	14 (36 %)	8.51 (18 %)	14 (41 %)	13 (44 %)	11 (33 %)	14 (49 %)
	NEI_monthly	12 (31 %)	5.88 (12 %)	7.66 (23 %)	7.80 (25 %)	5.88 (18 %)	9.61 (34 %)
	NEI_hourly	13 (34 %)	6.68 (14 %)	7.36 (19 %)	7.89 (26 %)	5.00 (15 %)	8.83 (31 %)
Surface CO [ppb]							
r_s	BASE	0.11	0.10	0.36	0.22	0.33	0.16
	NEI_monthly	0.12	0.11	0.45	0.25	0.43	0.39
	NEI_hourly	0.14	0.08	0.48	0.34	0.43	0.36
MBE (%)	BASE	-85 (-35%)	-27 (-14%)	-71 (-28 %)	-70 (-27 %)	-44 (-18 %)	-136 (-46 %)
	NEI_monthly	-61 (-25 %)	-1.47 (-0.8 %)	-45 (-18 %)	-51 (-20 %)	-5.12 (-2.1 %)	-71 (-24 %)
	NEI_hourly	0.04 (0.02 %)	52 (28 %)	-34 (-14 %)	-30 (-12 %)	-31 (-13 %)	-90 (-31 %)
RMSE (%)	BASE	153 (63 %)	146 (79 %)	130 (52 %)	154 (60 %)	114 (47 %)	222 (76 %)
	NEI_monthly	148 (61 %)	153 (83 %)	111 (44 %)	138 (53 %)	112 (47 %)	185 (63 %)
	NEI_hourly	159 (65 %)	184 (99 %)	109 (43 %)	130 (50 %)	111 (46 %)	193 (66 %)
NO ₂ VCD _{Trop} [molecules/cm ²]							
r_s	BASE	0.79	0.65	0.77	0.75	0.85	0.71
	NEI_monthly	0.69	0.61	0.75	0.74	0.83	0.70
	NEI_hourly	0.74	0.63	0.75	0.75	0.83	0.70
MBE (%)	BASE	-2.87e+14 (-30%)	-2.67e+14 (-29 %)	-2.62e+14 (-25 %)	-2.67e+14 (-27 %)	-3.03e+14 (-31 %)	-3.21e+14 (-32 %)
	NEI_monthly	-3.68e+14 (-39 %)	-3.49e+14 (-38 %)	-3.55e+14 (-34 %)	-3.55e+14 (-35 %)	-3.90e+14 (-39 %)	-3.88e+14 (-39 %)
	NEI_hourly	-3.30e+14 (-35 %)	-3.23e+14 (-35 %)	-3.49e+14 (-34 %)	-3.49e+14 (-35 %)	-3.97e+14 (-40 %)	-3.93e+14 (-40 %)
RMSE (%)	BASE	4.80e+14 (50 %)	3.30e+14 (36 %)	3.10e+14 (30 %)	3.20e+14 (32 %)	3.70e+14 (37 %)	3.60e+14 (37 %)
	NEI_monthly	5.70e+14 (60 %)	4.10e+14 (45 %)	4.00e+14 (38 %)	4.10e+14 (40 %)	4.60e+14 (47 %)	4.20e+14 (43 %)
	NEI_hourly	5.30e+14 (56 %)	3.80e+14 (42 %)	3.90e+14 (38 %)	4.00e+14 (40 %)	4.70e+14 (47 %)	4.30e+14 (43 %)
HCHO VCD _{Trop} [molecules/cm ²]							

r_s	BASE	0.75	0.60	0.69	0.92	0.75	0.90
	NEI_monthly	0.75	0.60	0.69	0.92	0.76	0.89
	NEI_hourly	0.75	0.60	0.68	0.92	0.75	0.90
MBE (%)	BASE	1.40e+15 (18 %)	2.19e+15 (28 %)	2.52e+15 (27 %)	3.73e+15 (32 %)	1.99e+15 (22 %)	2.11e+15 (23 %)
	NEI_monthly	1.16e+15 (15 %)	1.97e+15 (25 %)	2.20e+15 (23 %)	3.34e+15 (29 %)	1.64e+15 (18 %)	2.09e+15 (23 %)
	NEI_hourly	1.28e+15 (16 %)	2.05e+15 (26 %)	2.18e+15 (23 %)	3.38e+15 (29 %)	1.56e+15 (17 %)	2.02e+15 (22 %)
RMSE (%)	BASE	3.10e+15 (40 %)	2.90e+15 (37 %)	3.10e+15 (33 %)	4.40e+15 (39 %)	2.70e+15 (30 %)	2.90e+15 (31 %)
	NEI_monthly	3.00e+15 (38 %)	2.80e+15 (36 %)	2.80e+15 (30 %)	4.00e+15 (34 %)	2.30e+15 (26 %)	2.80e+15 (30 %)
	NEI_hourly	3.10e+15 (39 %)	2.90e+15 (37 %)	2.80e+15 (30 %)	4.00e+15 (35 %)	2.30e+15 (25 %)	2.70e+15 (29 %)
CO VCD _{Total} [molecules/cm ²]							
r_s	BASE	0.53	0.37	0.26	0.53	0.11	0.20
	NEI_monthly	0.53	0.36	0.28	0.52	0.12	0.13
	NEI_hourly	0.54	0.35	0.26	0.52	0.12	0.15
MBE (%)	BASE	-2.76e+16 (-1.8 %)	2.65e+16 (1.8 %)	-9.24e+16 (-5.4 %)	1.35e+17 (8.5 %)	-1.78e+17 (-10 %)	6.89e+16 (4.3 %)
	NEI_monthly	-3.79e+16 (-2.5 %)	4.75e+15 (0.3 %)	-1.19e+17 (-7.0 %)	1.14e+17 (7.2 %)	-1.87e+17 (-11 %)	7.63e+16 (4.8 %)
	NEI_hourly	-1.85e+16 (-1.2 %)	2.64e+16 (1.8 %)	-1.11e+17 (-6.5 %)	1.27e+17 (8.0 %)	-1.93e+17 (-11 %)	7.23e+16 (4.5 %)
RMSE (%)	BASE	2.60e+17 (17 %)	1.90e+17 (13 %)	2.1e+17 (12 %)	2.4e+17 (15 %)	3.30e+17 (19 %)	3.10e+17 (19 %)
	NEI_monthly	2.60e+17 (17 %)	1.80e+17 (13 %)	2.2e+17 (13 %)	2.3e+17 (14 %)	3.40e+17 (19 %)	3.20e+17 (20 %)
	NEI_hourly	2.60e+17 (17 %)	1.90e+17 (13 %)	2.1e+17 (12 %)	2.4e+17 (15 %)	3.40e+17 (19 %)	3.20e+17 (20 %)

Table S3. Same as Table S2 but for surface concentrations of SO₂ and PM_{2.5}. Comparison of July mean values from SLAMS observations and MUSICA model simulations across six regions.

	Region /Simulation ID	West Coast	Mountain	Midwest	Southwest	Northeast	Southeast
Surface SO ₂ [ppb]							
r_s	Base	0.41	-0.09	0.00	0.14	0.32	0.13
	NEI_monthly	0.41	0.15	-0.06	-0.05	0.13	0.02
	NEI_hourly	0.43	0.11	-0.03	-0.06	0.12	-0.01
MBE (%)	Base	2.71 (361 %)	0.91 (98 %)	4.99 (683 %)	2.78 (353 %)	11 (1651 %)	3.94 (861 %)
	NEI_monthly	-0.56 (-74 %)	-0.57 (-62 %)	-0.14 (-20 %)	0.04 (5.5 %)	-0.34 (-49 %)	-0.29 (-64 %)
	NEI_hourly	-0.51 (-68%)	-0.54 (-58 %)	-0.12 (-16 %)	0.15 (20 %)	-0.33 (-48 %)	-0.28 (-61 %)
RMSE (%)	Base	4.66 (621 %)	3.19 (343 %)	9.52 (1303 %)	3.96 (502 %)	20 (2866 %)	7.35 (1607 %)
	NEI_monthly	1.12 (149 %)	1.14 (122 %)	1.05 (144 %)	1.66 (210 %)	0.86 (125 %)	0.81 (178 %)
	NEI_hourly	1.11 (147 %)	1.13 (122 %)	1.06 (145 %)	1.74 (221 %)	0.86 (125 %)	0.81 (178 %)
Surface PM _{2.5} [µg/m3]							
r_s	Base	0.43	0.32	0.75	-0.35	0.15	0.27
	NEI_monthly	0.38	0.30	0.76	-0.26	0.06	0.39
	NEI_hourly	0.38	0.29	0.72	-0.30	0.08	0.41
MBE (%)	Base	5.07 (52 %)	-2.38 (-31 %)	-1.03 (-13 %)	-2.25 (-16 %)	3.19 (36 %)	3.20 (37 %)
	NEI_monthly	4.69 (48 %)	-2.55 (-33 %)	-1.72 (-22 %)	-2.90 (-21 %)	2.20 (25 %)	2.34 (27 %)
	NEI_hourly	5.35 (55 %)	-2.14 (-27 %)	-1.31 (-16 %)	-2.61 (-19 %)	2.53 (29 %)	2.52 (29 %)
RMSE (%)	Base	9.66 (99 %)	3.77 (49 %)	2.37 (30 %)	5.92 (43 %)	4.14 (47 %)	4.09 (47 %)
	NEI_monthly	9.46 (97 %)	3.87 (50 %)	2.59 (32 %)	5.89 (42 %)	3.68 (42 %)	3.11 (36 %)
	NEI_hourly	9.82 (100 %)	3.67 (47 %)	2.41 (30 %)	5.84 (42 %)	3.93 (45 %)	3.23 (37 %)

Table S4. Summary of the observational datasets used for MUSICA model evaluation. The table shows the units used in our analysis, which may differ from those in the original data sources.

Dataset/ Instrument	Variable [unit]	Data Type	Temporal Resolution	Spatial Resolution	Availability	Domain/Sites	Data Source
State and Local Monitoring Stations (SLAMS)	O ₃ [ppb] NO ₂ [ppb] CO [ppb] SO ₂ [ppb] PM _{2.5} [µg/m ³]	Surface Measurement	Hourly	Not applicable	1980-Present	CONUS	AQS Air Data (https://aqs.epa.gov/aqswweb/airdata/download_files.html ; access date: 8/1/2023)
Level-2 TROPOMI RPRO Version 02.04.00	HCHO [molec/cm ²] and Averaging Kernels [unitless]	Tropospheric VCD Retrievals	Daily (~1:30 PM Local Time)	5.5 km x 3.5 km (Re-gridded to 0.15° x 0.15° selecting for QA>0.75)	5/7/2018- Present	Global	GES DISC (doi: 10.5270/S5P-vg1i7t0; access date: 12/1/2023)
Level-2 TROPOMI RPRO Version 02.04.00	NO ₂ [molec/cm ²] and Averaging Kernels [unitless]	Tropospheric VCD Retrievals	Daily (~1:30 PM Local Time)	5.5 km x 3.5 km (Re-gridded to 0.15° x 0.15° selecting for QA>0.75)	5/1/2018- Present	Global	GES DISC (doi: 10.5270/S5P- 9bnp8q8; access date: 12/1/2023)
Level-2 TROPOMI RPRO Version 02.04.00	CO [molec/cm ²] and Averaging Kernels [unitless]	Tropospheric VCD Retrievals	Daily (~1:30 PM Local Time)	5.5 km x 7 km (Re-gridded to 0.15° x 0.15° selecting for QA>0.75)	4/30/2018- Present	Global	GES DISC (doi: 10.5270/S5P-bj3nry0; access date: 12/1/2023)

Table S5. Geographical locations of the six selected State and Local Monitoring Stations (SLAMS) marked on Fig. 1.

City	Region	Site Name	AQS Site ID	Latitude	Longitude
Los Angeles	WestCoast	Los Angeles - North Main Street (CA)	06-037-1103	34.06659	-118.22688
Denver	Mountain	Denver - CAMP (CO)	08-031-0002	39.751184	-104.98763
Chicago	Midwest	Chicago - Naperville-Elgin (IL)	17-031-3103	41.965193	-87.876265
Houston	Southwest	Houston - Bayland Park (TX)	48-201-0055	29.695729	-95.499219
New York City	Northeast	New York - Queens College (NY)	36-081-0124	40.73614	-73.82153
Atlanta	Southeast	Atlanta - South DeKalb (GA)	13-089-0002	33.6878	-84.2905

REFERENCES

- Davis, N. A., Callaghan, P., Simpson, I. R., and Tilmes, S.: Specified Dynamics Scheme Impacts on Wave-Mean Flow Dynamics, Convection, and Tracer Transport in CESM2 (WACCM6), *Atmos Chem Phys*, 22, 197–214, <https://doi.org/10.5194/acp-22-197-2022>, 2022.
- Gaubert, B., Emmons, L. K., Raeder, K., Tilmes, S., Miyazaki, K., Arellano Jr., A. F., Elguindi, N., Granier, C., Tang, W., Barré, J., Worden, H. M., Buchholz, R. R., Edwards, D. P., Franke, P., Anderson, J. L., Saunio, M., Schroeder, J., Woo, J.-H., Simpson, I. J., Blake, D. R., Meinardi, S., Wennberg, P. O., Crouse, J., Teng, A., Kim, M., Dickerson, R. R., He, H., Ren, X., Pusede, S. E., and Diskin, G. S.: Correcting Model Biases of CO in East Asia: Impact on Oxidant Distributions During Korus-Aq KORUS-AQ, *Atmos Chem Phys*, 20, 14617–14647, <https://doi.org/10.5194/acp-20-14617-2020>, 2020.
- Li, J., Yu, S., Chen, X., Zhang, Y., Li, M., Li, Z., Song, Z., Liu, W., Li, P., Xie, M., and Xing, J.: Evaluation of the WRF-CMAQ Model Performances on Air Quality in China with the Impacts of the Observation Nudging on Meteorology, *Aerosol Air Qual Res*, 22, 220023, <https://doi.org/10.4209/aaqr.220023>, 2022.
- van Noije, T. P. C., Eskes, H. J., van Weele, M., and van Velthoven, P. F. J.: Implications of the Enhanced Brewer-Dobson Circulation in European Centre for Medium-Range Weather Forecasts Reanalysis Era-40 for the Stratosphere-Troposphere Exchange of Ozone in Global Chemistry Transport Models, *Journal of Geophysical Research: Atmospheres*, 109, <https://doi.org/10.1029/2004JD004586>, 2004.
- Otte, T. L.: The Impact of Nudging in the Meteorological Model for Retrospective Air Quality Simulations. Part I: Evaluation against National Observation Networks, *J Appl Meteorol Climatol*, 47, 1853–1867, <https://doi.org/10.1175/2007JAMC1790.1>, 2008.
- Schwantes, R. H., Lacey, F. G., Tilmes, S., Emmons, L. K., Lauritzen, P. H., Walters, S., Callaghan, P., Zarzycki, C. M., Barth, M. C., Jo, D. S., Bacmeister, J. T., Neale, R. B., Vitt, F., Kluzek, E., Roozitalab, B., Hall, S. R., Ullmann, K., Warneke, C., Peischl, J., Pollack, I. B., Flocke, F., Wolfe, G. M., Hanisco, T. F., Keutsch, F. N., Kaiser, J., Bui, T. P. V, Jimenez, J. L., Campuzano-Jost, P., Apel, E. C., Hornbrook, R. S., Hills, A. J., Yuan, B., and Wisthaler, A.: Evaluating the Impact of Chemical Complexity and Horizontal Resolution on Tropospheric Ozone Over the Conterminous US With a Global Variable Resolution Chemistry Model, *J Adv Model Earth Syst*, 14, e2021MS002889, <https://doi.org/10.1029/2021MS002889>, 2022.